Technical Note	LIGO-T1800200–v4	2018/10/30

In Situ Laser Mode Spectroscopy for Mirror Phase Mapping

Sandrine Ferrans

Mentors: Rana Adhikari, Koji Arai, and Gautam Venugopalan

1 Abstract

The LIGO detectors are Michelson based interferometers with Fabry Perot cavities. The Fabry Perot cavities in aLIGO creates an optical resonator with semi-transparent spherical mirrors, where light is reflected and transmitted before being merged into an interference pattern for output. However, the mirrors are not perfect and contain surface defects which contribute to optical losses. This project is focused on improving the optics in LIGO by characterizing mirror figure error that contribute to optical losses. As a result of scattered light, optical losses increase shot noise and destroy the squeeze state of light. Surface perturbations will be evaluated with In-Situ mode spectroscopy, so the gravitational wave output will not be affected. Mirror figure error will cause the resonant frequencies of the Hermite Gaussian modes to shift from their ideal theoretical spacings. Mirror phase maps, a physical representation of the mirror, can be reconstructed by analyzing the shift in transverse mode spacings with Bayesian inference techniques. The success of aLIGO is largely due to precise optical measurements. By mapping the physical surface of the mirror down to 1 Angstrom, the surface perturbations contributing to optical losses will be mapped.

2 Introduction

2.1 Gravitational Waves

Einstein predicted gravitational waves in his theory of General Relativity, which states that gravity is the distortion of spacetime due to the presence of mass. Mass creates a curvature in the geometry of spacetime. Gravitational waves are ripples in the fabric of spacetime, and these waves distort spacetime geometry as they propagate at the speed of light. Gravitational waves interact with matter by stretching in one direction and compressing space in the perpendicular direction. They originate from the acceleration of large masses, specifically from cataclysmic cosmic events such as the collision of black holes. Gravitational waves are important because they carry information about their origin, the universe, and the nature of gravity itself.

2.2 LIGO

LIGO (Laser Interferometer Gravitational Wave Observatory) is a gravitational wave detector in Livingston, Louisiana, and in Hanford, Washington. LIGO is a Michelson based interferometer with Fabry Perot cavities. The interferometer creates an interference pattern from the constructive or deconstructive interference of waves. The interferometer has two perpendicular arms of equal length. The laser beam will take the same time to travel the same distance, which will produce deconstructive interference, where the light waves cancel each other out. Thus, the photodetector will not detect a light pattern. However, when a gravitational wave passes, the length of the arms changes. One arm is stretched, and the other one is compressed. The photodetector will detect an interference pattern due to the changes in relative length between the masses. Gravitational waves will alter the time the light will travel in the interferometer. The difference in time will produce an interference pattern in which astronomical information can be extracted.
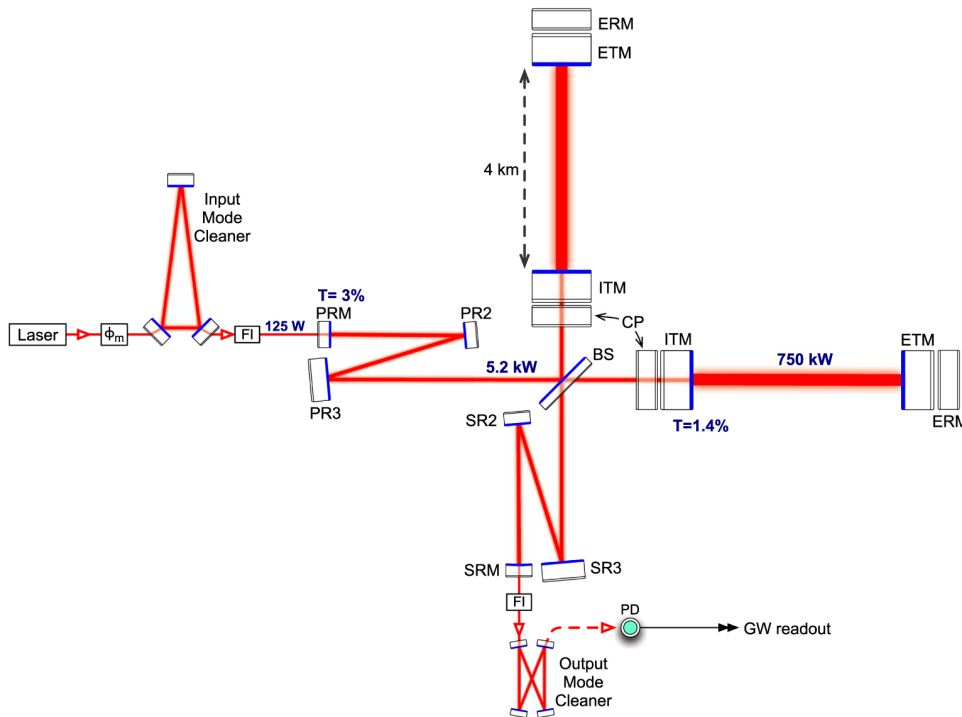
Figure 1: Schematic diagram of Advanced LIGO

The arms of LIGO are 4 km long. Incorporating Fabry Perot cavities into each arm increases the sensitivity by increasing the interaction time of the gravitational wave with the interferometer. This can be done by introducing additional mirrors near the beam splitter, causing the each part of the laser beam to reflect 280 times before being merged into an interference pattern [1]. However, increasing the amount of reflections can introduce optical losses in the laser.

2.3 Optical Losses

The success of Advanced LIGO is largely due to precise optical measurements which result in the sensitivity to detect gravitational waves. This project is focused on improving the optics in LIGO by characterizing mirror figure error that contribute to optical losses. Optical losses are a result of light scattering. Defects, absorption, microroughness, transmission by the end test mass, and mirror figure error cause light scattering. Mirror figure error has a low spatial frequency, which causes a low scattering angle of light. [2].

The project is aimed to reduce optical power losses due to mirror figure error. The requirements of Advanced LIGO are that the round trip cavity loss must be less than 75 parts per million [3]. Mirror figure error is the second largest contributor to optical losses, with a budget of 24 ppm for the combination of both test masses [3]. Optical losses destroy the squeezed state of light, reduce the circulating power in the cavities, which increases shot noise. Most importantly, scattered light alters the phase of the laser, which is ultimately what LIGO uses to detect gravitational waves. Thus, it is highly important for LIGO to reduce optical losses in order to achieve the sensitivity to detect gravitational waves.
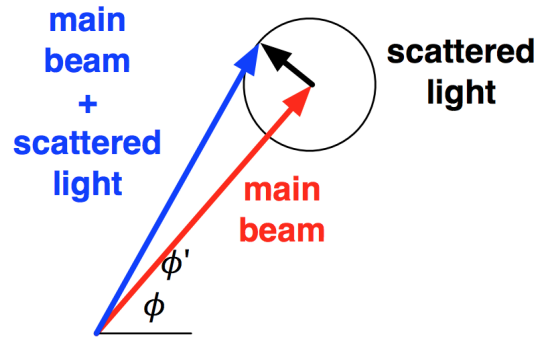
Figure 2: The effect of scattered light.

An in-situ technique to characterize mirror figure error using an optical cavity was demonstrated on 40m prototype gravitational wave detector. Ultimately, we will measure the transverse mode spacings and create mirror phase maps from analyzing the shift in spacings. Mirror maps are conventionally created using Fizeau interferometry. However, Fizeau interferometry does not have high precision and would effect the gravitational wave detector's output, Thus, we will use an in-situ technique in order to see what the interferometric beam sees.

2.4 Optical Resonators

2.4.1 Fabry Perot Cavity

An optical resonator is a system that consists of two mirrors that form a standing wave. A cavity eigenmode describes the standing wave pattern, which is the light pattern that is continuously reflected. Only certain modes are allowed to resonate inside of the cavity.

The Fabry Perot cavity used in Advanced LIGO is an optical resonator with spherical mirrors. There are two types of modes: longitudinal modes and transverse modes. Longitudinal modes describe the laser frequency and determine the certain frequencies that are allowed to resonant inside of the cavity. Longitudinal modes are determined by the absolute length of the cavity. A transverse mode differs in frequency and amplitude, and it depends on the radius of the curvature of the mirrors. The Fabry Perot cavity in LIGO is composed of the input test mass (ITM) and the end test mass (ETM). The ITM is a flat mirror, and the ETM is a spherical mirror.

A Fabry Perot cavity has the following characteristics:

- E_i is the incident electric field,

- E_t represents transmitted electric field,

- The reflected electric field is E_r,

For an ideal cavity, the electric field inside of the cavity is:
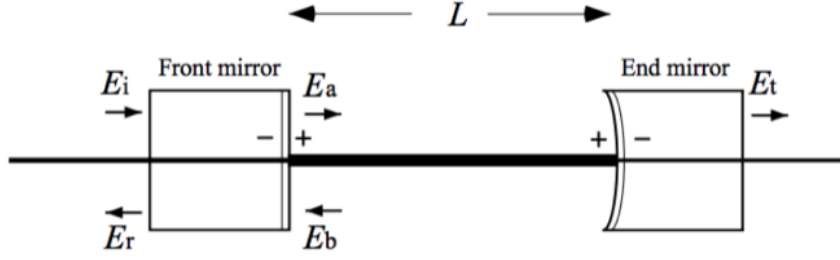
Figure 3: A Fabry Perot Cavity source:[9]

$$E_a = t_I E_i + r_I E_b$$

$$E_b = r_E e^{i\frac{2L\Omega}{c}} E_a$$

The reflected electric field E_r and the transmitted electric field E_t are given by,

$$E_r = -r_E E_i + t_I E_b$$

$$E_t = t_E e^{-i\frac{L\Omega}{c}} E_a$$

Where Ω is the angular frequency of the incident beam,

The ITM and ETM have the following reflectivity and transmissitivity,

- The reflectivity of the ITM, $R_I = r_I^2$,

- The reflectivity of the ETM, $R_E = r_E^2$,

- The transmissivity of the ITM, $T_I = t_I^2$,

- The transmissivity of the ETM, $T_E = t_E^2$,

The reflectivity and of the cavity are given by,

$$r_{cav} = \frac{E_r}{E_i} = -r_I + \frac{t_I^2 r_E e^{-i\phi}}{1 - r_F r_E e^{-i\phi}}$$

$$t_{cav} = \frac{E_t}{E_i} = \frac{t_I t_E e^{\frac{-i\phi}{2}}}{1 - r_I r_E e^{-i\phi}}$$

The roundtrip phase shift of the cavity, $\phi = \frac{2L\Omega}{c}$

The power P is proportional to the magnitude of the electric field, $P = |E|^2$

The following equation describes the transmitted light intensity,

$$P_t = \frac{I}{I_0} = \frac{t_I t_E e^{\frac{-i\phi}{2}}}{1 - r_I r_E e^{-i\phi}}$$

In an ideal Fabry Perot with no optical losses, the sum of reflectivity and transmissivity of a mirror are equal to 1.

$$R + T = 1$$

However, when optical losses, L, are present:

$$R + T + L = 1$$

A system with perfectly spherical mirrors has Gaussian modes. A Gaussian mode is a transverse mode, and the intensity of light can be described in a Gaussian distribution function. The fundamental Gaussian mode has repetitive resonances with the laser frequency of the Free Spectral Range (FSR), which describes the spaces between two resonant longitudinal modes. The FSR is defined as,

$$\nu_{FSR} = \frac{c}{2L} = 3.7474 \times 10^6 Hz \tag{1}$$

The FSR is determined by the absolute length of the cavity. The FSR is known as the fundamental mode of resonance or TEM_{00}.

2.4.2 Hermite Gaussian Modes

A Hermite Gaussian mode is a higher order mode that has an intensity distribution that differs from the fundamental Gaussian mode. Hermite Gaussian modes are described by spacial indices (n,m) for TEM_{nm}. Hermite Gaussian modes describe electrical field distributions, composed of a Hermite Polynomial and a Gaussian function.

$$E_{nm}(x,y,z) = E_0 \frac{w_0}{w(z)} H_n\left(\frac{\sqrt{2}x}{w(z)}\right) H_m\left(\frac{\sqrt{2}y}{w(z)}\right) \exp\left(-\frac{x^2+y^2}{w(z)^2}\right) \exp\left(-i\left[kz - (1+n+m)\arctan\left(\frac{z}{z_R}\right)\right]\right)$$

$$\tag{2}$$

Where:

- E_0 is the electric field amplitude,

- H_n is the nth order polynomial,

- W_0 represents the beam waist,

- $W(z)$ is the beam radius along the z-axis,

- $R(z)$ represents the radius of curvature of the wavefront,

- z_R is the distance along the z-axis where the wavefronts of the beam are most curved.

The Hermite Gaussian modes as a representation of the electric field distributions of a beam are analogous to the energy perturbations in a simple quantum harmonic oscillator. The energy in a harmonic oscillator is composed of a one dimensional Hermite polynomial, and the electric field amplitudes of a beam is a two dimensional problem with two Hermite polynomials.
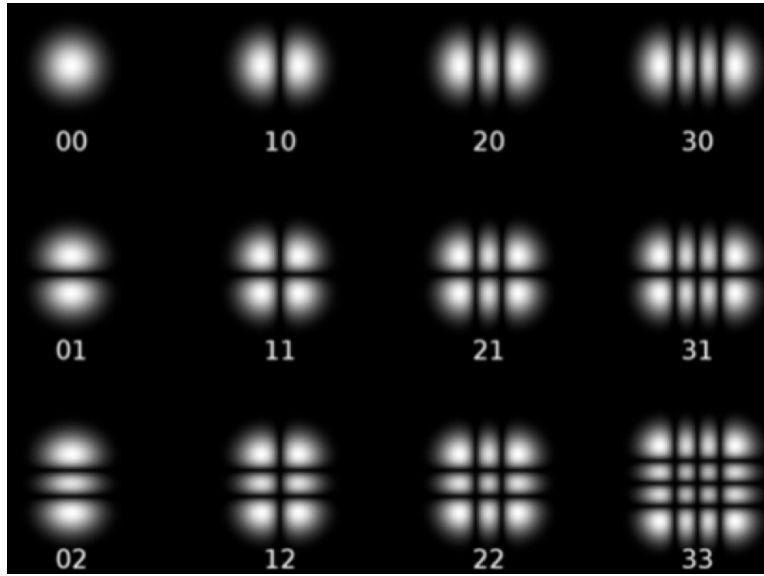

Figure 4: Hermite Gaussian Modes

The Transverse Mode Spacing (TMS) is the distance between transverse modes. The higher order modes have a frequency separation of multiples of the transverse mode spacing from the fundamental mode of resonance.

$$\nu_{TMS} = \nu_{FSR} \times \left(\tfrac{n+m}{\pi}\right) \cos^{-1} \sqrt{g_1 g_2}$$

Mirror figure error causes a shift in the transverse mode spacings. Thus, information about mirror figure error will be extracted by precisely measuring the shift of the transverse mode frequencies.

The g parameters depend on the absolute length of the cavity and the radius of curvature of the mirrors.

$$g_1 = 1 - \tfrac{L}{R_1} \approx 1$$

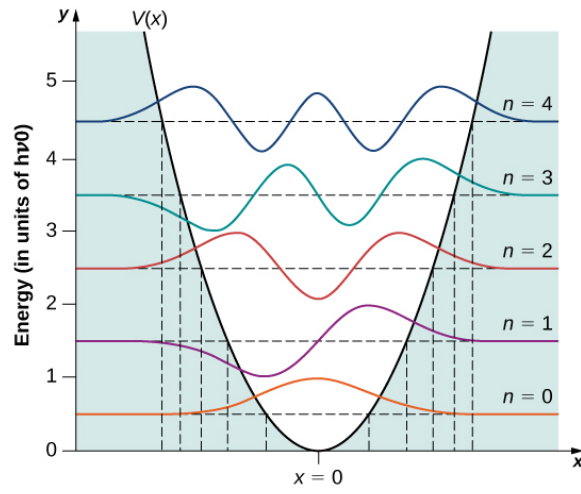$$g_2 = 1 - \tfrac{L}{R_2} \approx 0.298$$
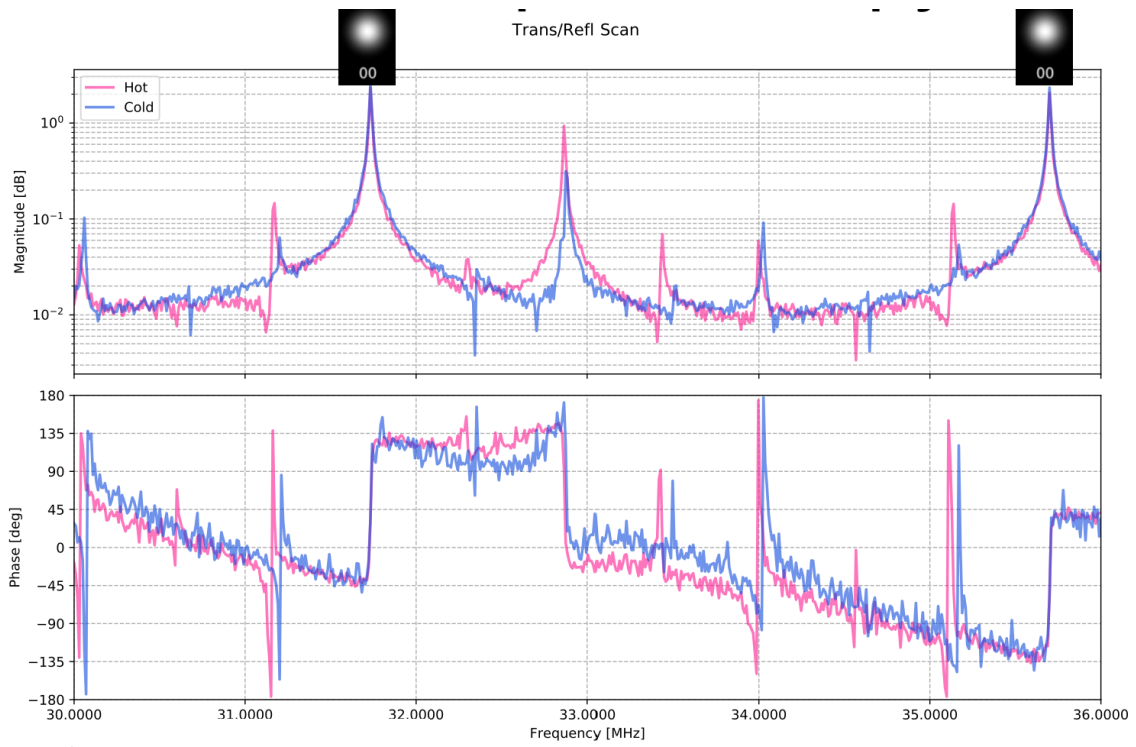
Figure 5: Energy Levels of a Harmonic Oscillator

Figure 6: Frequency scan showing the shift in TMS

The Gouy Phase is $\Delta\varphi$,

$$\Delta\varphi = \varphi(z_2) - \varphi(z_1) = \cos^{-1}\pm\sqrt{g_1 g_2}. \tag{3}$$

The Gouy Phase is stronger for HOMs, which can cause the resonant frequencies to be higher.

3   Objectives

- Perform in-situ mode spectroscopy on the 40m LIGO prototype interferometer by injecting an additional (AUX) laser.

- Insert a heater into the ETMY to create a known deformation in the mirror and to make the experimental set up more sensitive to HOMs.

- Use Finesse software to simulate mirror figure error with the use of Zernike Polynomials and study the theoretical cavity scan.

- Use frequency scan data from experiment and Finesse to run the Markov Chain Monte Carlo method in order to produce the most probable mirror phase maps.

The goal of this project is to create a mirror map that characterizes the figure error on the test masses causing optical losses.

4   Experimental Methods

4.1   In-Situ Mode Spectroscopy

Mode spectroscopy is a technique to measure the frequency of a laser and its higher order modes. This will be performed with an in-situ technique using an auxiliary laser (AUX) in 40m prototype interferometer in order to measure mode spacings. Therefore the interferometer will consist of the two beams: the pre stabilized laser (PSL), which is the beam that is used for the detection of gravitational waves, and the auxiliary laser. It is important to note that the auxiliary laser will not disturb the output of the interferometer, and therefore this technique can be applied to aLIGO. An in-situ technique is critical to obtain a high precision mirror map in the interferometric beam's environment. The frequency of the AUX laser will be altered in order to produce many resonances.

Mode spectroscopy will be performed to measure the FSR and TMS. The FSR and TMS are determined by the frequency and the absolute length of the cavity. Thus, we rely on very accurate and precise measurements of the frequency and length of the cavity in order to determine the modes. However, the laser frequency and the arm cavity length are not stable enough to sustain the resonance of the cavity. Thus, feedback control will be used on either the frequency and the arm length using a Phase Lock Loop (PLL), and the Pound Drever Hall technique (PDH).

The goal of the PLL is to ensure that the PSL will resonate within the cavity and that the phase difference between the PSL and AUX is set. The PSL is locked using the Pound Drever Hall Locking, which stabilizes the laser by measuring the frequency with a Fabry Perot and feeding it back into the laser, ultimately suppressing frequency fluctuations [8]. The auxiliary laser will be injected from the optical port, and it will be locked to the Y arm of the interferometer. A beam splitter sends a small amount of the PSL and AUX beam to the PLL.
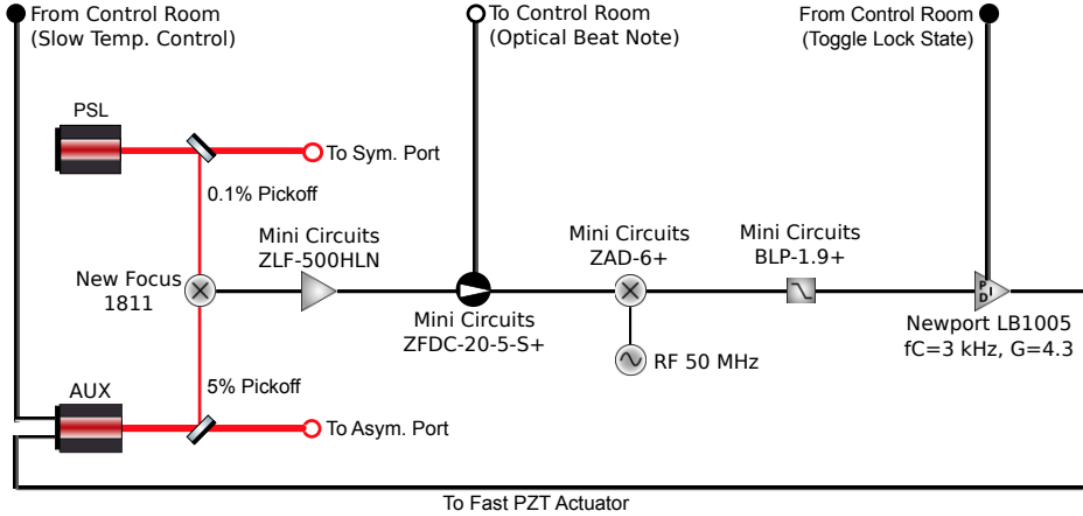

Figure 7: Schematic diagram of the AUX-PSL Phase locked loop

The electric field of the PSL and the AUX lasers with a power P and phase ϕ are respectively:

$$E_{PSL} \approx \sqrt{P_{PSL}}e^{-i\phi PSL(t)} \tag{4}$$

$$E_{AUX} \approx \sqrt{P_{AUX}}e^{-i\phi AUX(t)} \tag{5}$$

The marconi provides the RF signal, which sets the frequency difference between the lasers. A beat note is produced when both lasers undergo mixing.

$$P_{beat} \approx |E_{PSL} + E_{AUX}|^2 \tag{6}$$

The coupler sends part of the beat to the control room in order to monitor the beat frequency. The Phase Lock Loop will not lock if the beat frequency is not within a close range of the frequency set by the LO. The frequency of the beat can be altered if needed by changing the temperature of the laser. This will ensure that the PLL is in lock.

Resonance depends solely on the length cavity. If the length of the Fabry Perot cavity is unstable, then the PSL will adjust itself automatically to resonance.

Currently, we have developed multiple in-situ techniques to scan the frequency of the AUX laser:

- RF offset

- AOM sidebands

- Agilent Drive Signal

The RF offset produces cavity scans by sweeping the frequency of the AUX carrier and its sidebands. The RF offset changes carrier frequency (PSL). The RF frequency goes into the AOM. The AOM created two sidebands. The sidebands resonated with the FSR and the carrier, which resulted in too much power. It can be inferred that the repeated lines were higher order modes (HOM) due to the equal spacing. However, the frequency scan using the RF offset was unsuccessful because it was an incoherent measurement. The sidebands resonated with the FSR and the carrier, which resulted in too much power and over-saturation.

The goal of scanning the frequency using the AOM sidebands was to create a coherent and sentinel measurement. A transfer function will be created in order to measure the input power of the beam relative to the output of the beam at a specific frequency. This creates a pure measurement of the spectral power density. Therefore we are only looking at specific frequencies. The PSL is set to resonate within the cavity. The AOM creates two sidebands and sweeps outworks. However, the AOM sidebands technique was inconclusive because HOM's were unclear. Thus, we inserted a razor blade to add more power to the HOMs, but it was also unsuccessful. The photodetector (PD) measures the light going into the interferometer and the light after the AOM. Figure 8 shows the data obtained using the AOM sidebands.

The Agilent Drive Signal swept the AUX carrier frequency. The previous methods relied on the frequency of the AM sidebands being swept, and the carrier was locked at a fixed offset from the PSL carrier.

We used this method with a double demodulation, where the signal undergoes optical mixing twice, and then further simplified it further to a single demodulation.

Approximately $\frac{1}{3}$ of the output AUX beam was clipped by inserting a razor blade. This was done so the photodiode, PDA255, will witness more higher order modes by disrupting the symmetry of the output as seen in Figure 11.
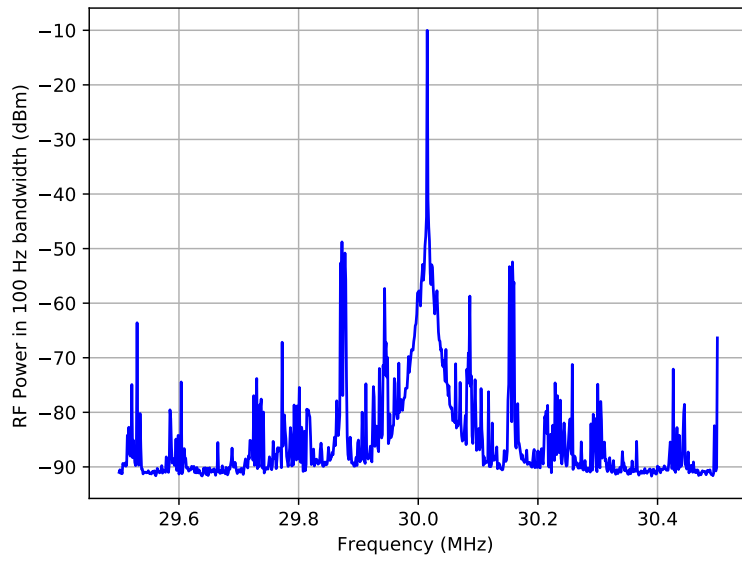
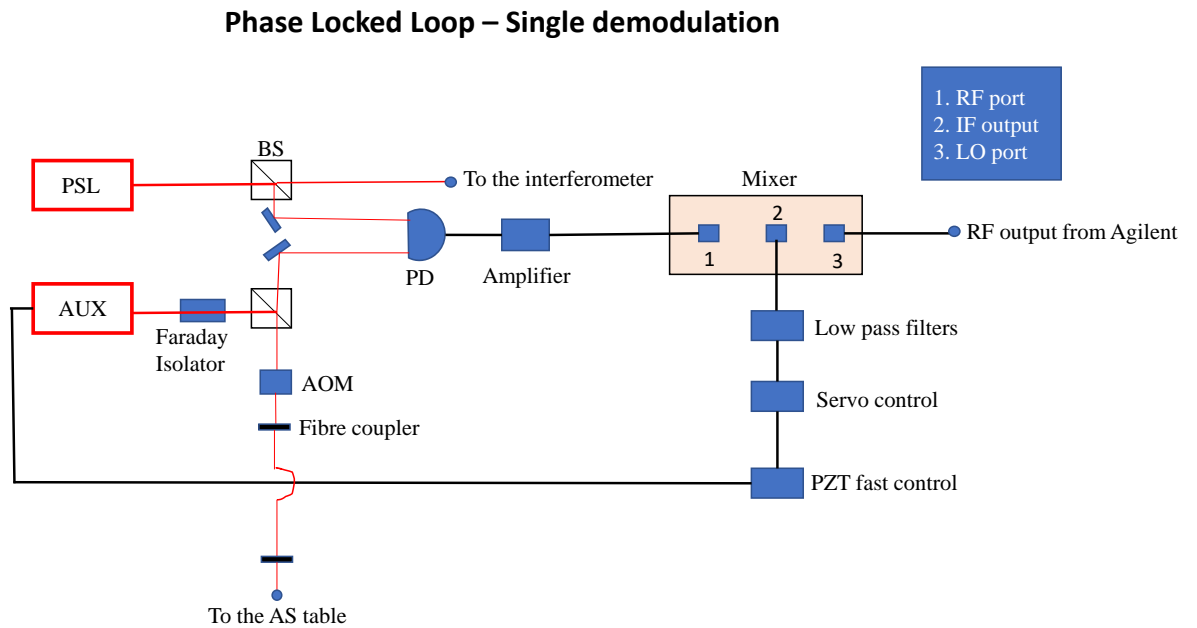Figure 8: Power Spectral Density using the AOM sidebands

Phase Locked Loop – Single demodulation

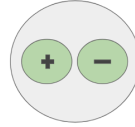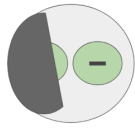Figure 9: The Agilent Drive technique with single demodulation

Unclipped TEM10

Figure 10: The phase of an unclipped beam

Clipped with Razorblade

Figure 11: The phase of a clipped beam, which disrupts the symmetry at the photodiode so it will witness more higher order modes.

4.2   The Use of a Heater for Mode Spectroscopy

Two heaters were installed to radiate electromagnetic radiation in the ETMY in order to create a known perturbation in the mirror and to make the set up more sensitive to higher order modes.

The transverse mode spacings depend on the radius of curvature of the mirrors. The heater will increase the radius of curvature of the mirror, and therefore decrease the transverse mode spacings.

It is important to note that each HOM will have a different beam size and will therefore witness a different radius of curvature.

The heater will be inserted into an elliptical reflector. However, the reflector will be half an ellipse to ensure that it does not block the laser beam path. The reflector is an ellipse because an ellipse has two focal points. The heater will be set at one focal point, so that the heat will be radiated towards the other focal point. The focal points will be a specific point on the ETM of the Y arm and this point will create a perturbation on the mirror. This is to focus all of the radiation and power into one point as precisely as possible.

The other heater installed in the ETMY chamber is a cylindrical heater, where the heat is focused onto two lenses. However, the heating power is very low.

The heating pattern produced by the elliptical reflector heater can be seen in Figure 12, and the heating pattern for the cylinder can be seen in Figure 13.

The ETMY chamber will have two heaters installed: an elliptical reflector and a cylinder with two lenses. These heaters will not be on at the same time. It is important to note that the deformations in the mirror are temporary. The following Figure 14 and Figure 15 show
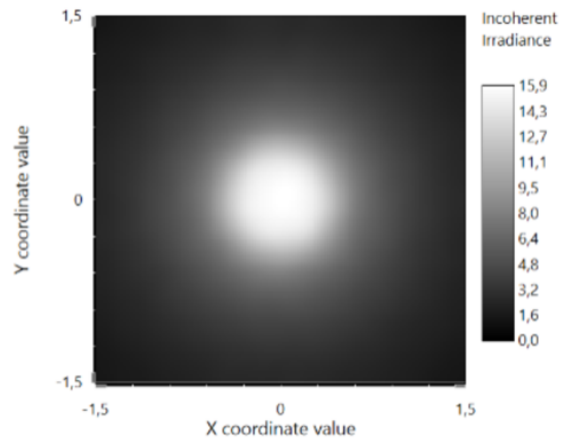
Figure 12: The heating pattern for the elliptical reflector heater.

Figure 13: The lens heating pattern.
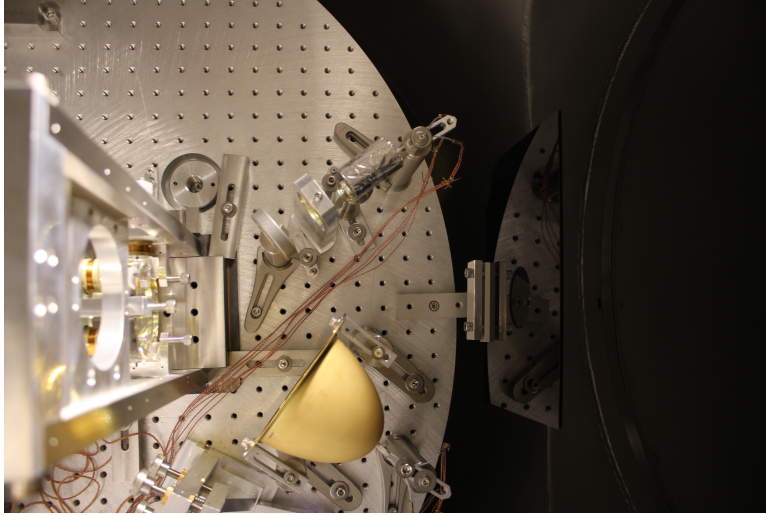
the set up in its entirety.

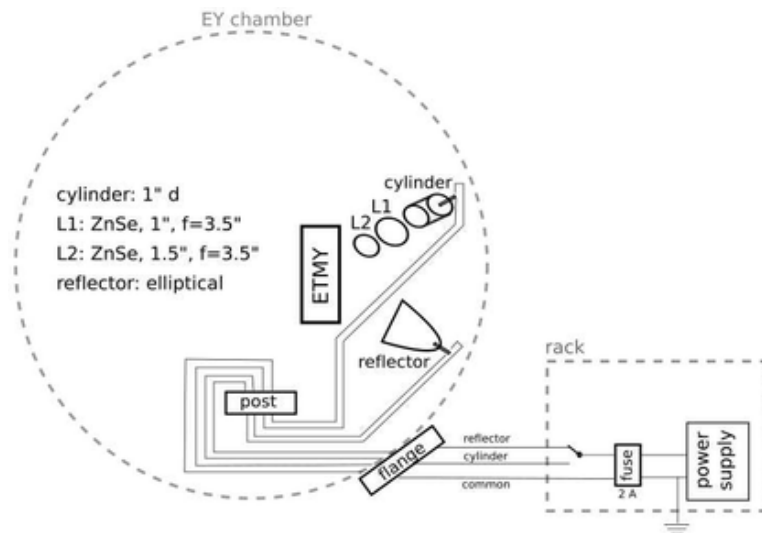Figure 14: A picture of the current heater set up in the vacuum chamber of ETMY.

Figure 15: Diagram showing both heaters inside the ETMY.

Table 1 and Table 2 describe the measurements taken with the heater set up.
Figure 16 and Figure 17 show a shift in TMS once the heating is applied.

Current (A)	Voltage (V)	Power (W)
0.5	3.4	1.7
0.6	5	3.0
0.8	9.4	7.5
0.9	12	10.8

Table 1: Measurements taken with an elliptical reflector heater

Current (A)	Voltage (V)	Power (W)
0.9	15	13.5

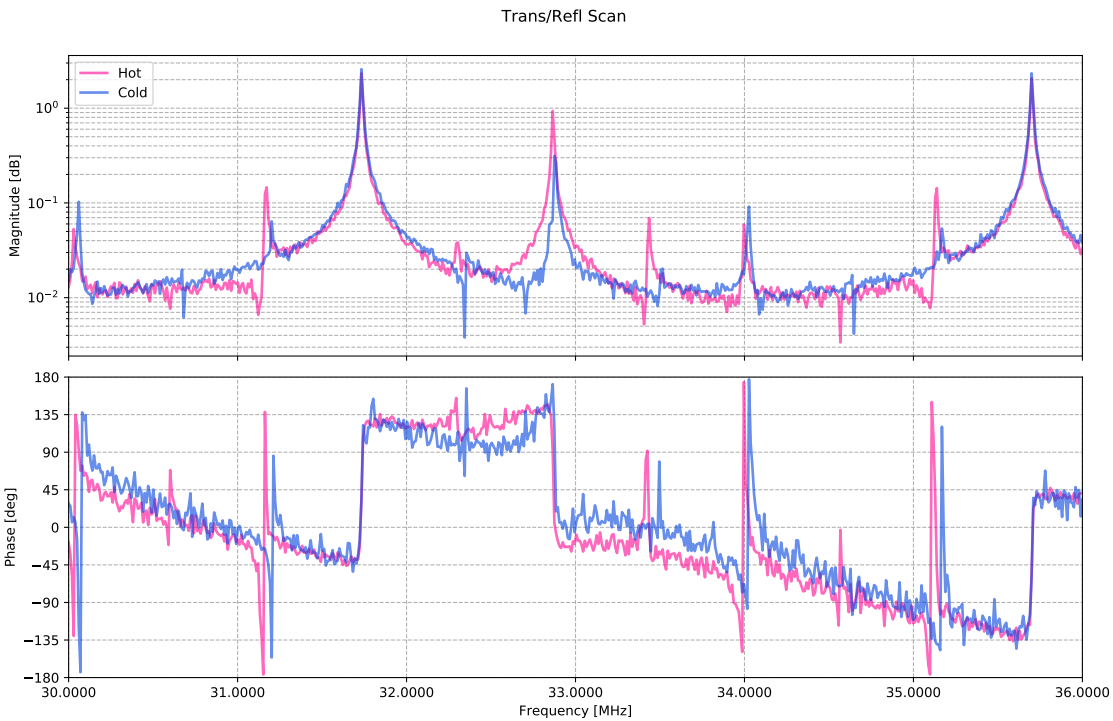Table 2: Measurements taken with a cylindrical heater

Figure 16: A total sweep of the laser frequency, where a shift in TMS can be observed after heating is applied.
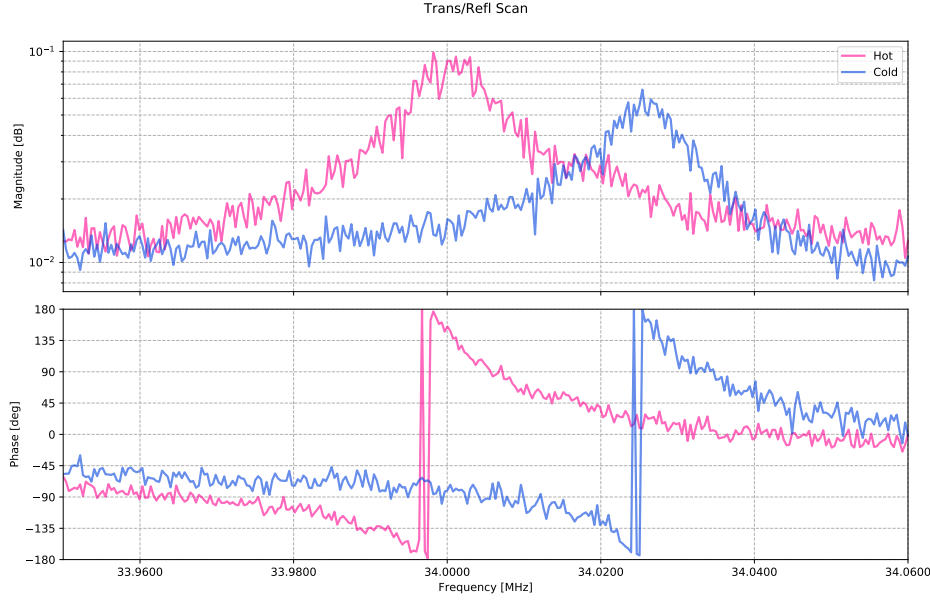
Trans/Refl Scan

Figure 17: Frequency scan for HOM 2 at a current of 0.9 A, which shows a shift in TMS.

5   Fitting the Data

5.1   Magnitude Fit

The magnitude data obtained from the cavity scan using the Agilent drive was fitted with the square root of a Lorentzian.

The magnitude data was fitted with the equation,

$$A\frac{B}{\sqrt{1 + \frac{X - C}{D}^2}} \tag{7}$$

- A is the constant background,

- B is the magnitude of the resonant peak,

- C is the central position of the peak,

- D is full width at half maximum.

The fitting equation was obtained from the transmitted power equation of a Fabry Perot cavity [5],

$$P_{off} + \frac{P}{\sqrt{1 + \frac{f - f_0^2}{f_c^2}}}$$

Mode	Cold State	Hot State (9A)
HOM 1	33.16 MHz	32.86 MHz
HOM 2	34.30 MHz	34.00 MHz
HOM 3	35.17 MHz	35.13 MHz
HOM 4	32.36 MHz	32.30 MHz
HOM 5	33.50 MHz	33.42 MHz

Table 3: Resonant Frequencies for each mode in cold and hot state.

C is the most important parameter because it contains information about how much the higher order modes shifted due to perturbations on the mirror. Figure 18 shows the fitting of HOM 1 with a current of 0.9 A.
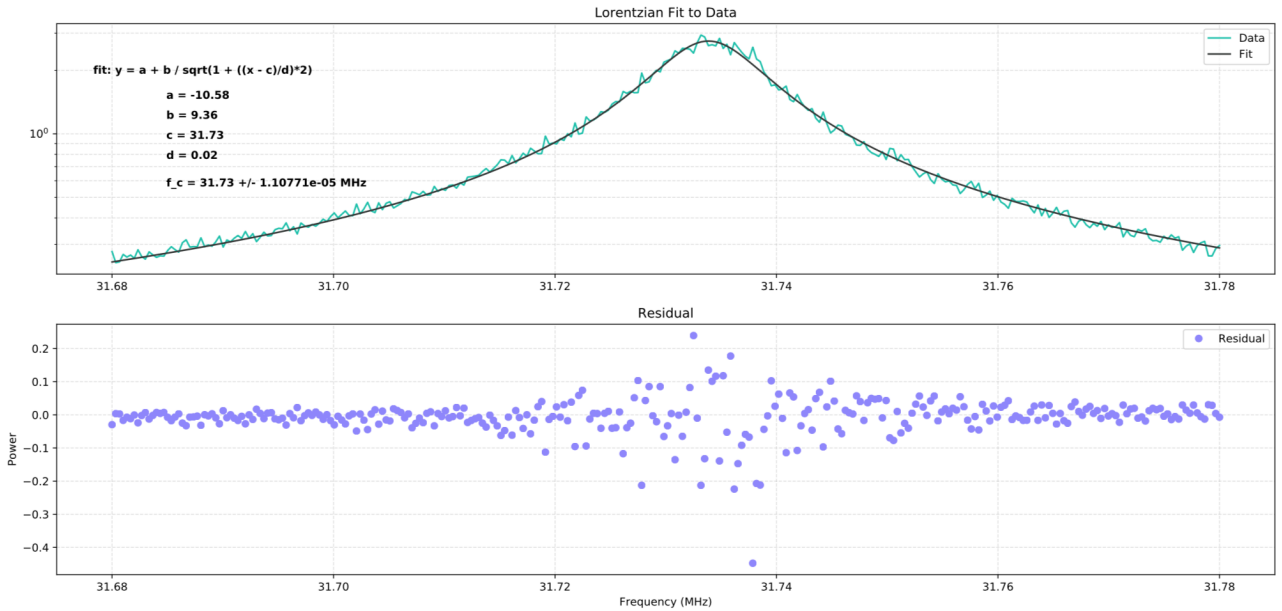

Figure 18: Fit for HOM 1 with elliptical reflector at 0.9 A

The fitting shows approximately 10 Hz of magnitude resolution.

The average of the resonant frequencies was calculated for the cold state and the hot state (9A) for the reflector to analyze the shift in frequencies in Table 3.

5.2   Complex Fit

The cavity scan information was obtained by measuring the magnitude and phase. Therefore, the magnitude and phase can be fitted simultaneously by reconstructing the data as a complex number, which will ultimately improve the fit.The magnitude is the real part Re, and the magnitude represents the imaginary part Im.

$$\frac{kjw^2}{\frac{w_0^2+jw_0}{Q-w^2}} \tag{8}$$

The complex reconstruction has the following properties:

- where k is the wavenumber,

- w0 is the resonance frequency,

- w represents the frequency,

- Q is the resonance frequency divided by the full width at half maximum. $Q = \frac{w_0}{FWHM}$
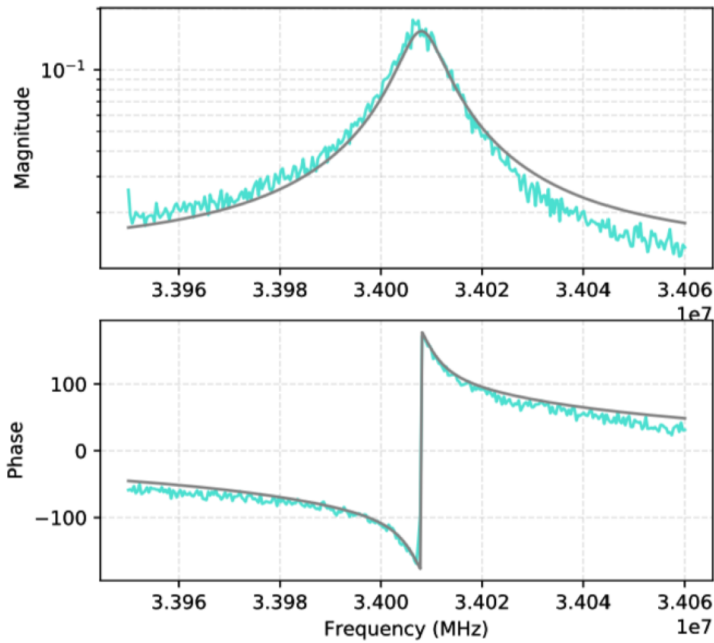
The complex fitting can be seen in Figure 19.

Figure 19: Fit for HOM 2 with elliptical reflector at 0.8 A

6   Finesse Simulations

Finesse (Frequency domain Interferometer SoftwarE) is an optical simulation software. An ideal Fabry Perot cavity will be simulated in Finesse. The ideal model will have no figure error and the same parameters as the 40m prototype interferometer as seen in Table 4. Its

Parameter	Value
Cavity length (L)	38.5 m
ITM Reflectivity (R)	0.98616
ITM Transmissivity (T)	0.01384
ETM Reflectivity (R)	0.9999863
ETM Transmissivity (T)	$1.37\text{x}10^{-6}$
ITM Radius of curvature (R_1)	∞
ETM Radius of curvature (R_2)	58 m

Table 4: Parameters of the 40m LIGO interferometer used for the Finesse simulation.

transverse mode spacings will be studied to create an ideal model and will be compared to the modes obtained experimentally to analyze the shift in the higher order modes.

Zernike polynomials will be used in Finesse to insert surface perturbations into the ETM. Zernike polynomials are characterized by their coefficients: the radial order n, and the angular order m, and they define the amplitude for a given mode.
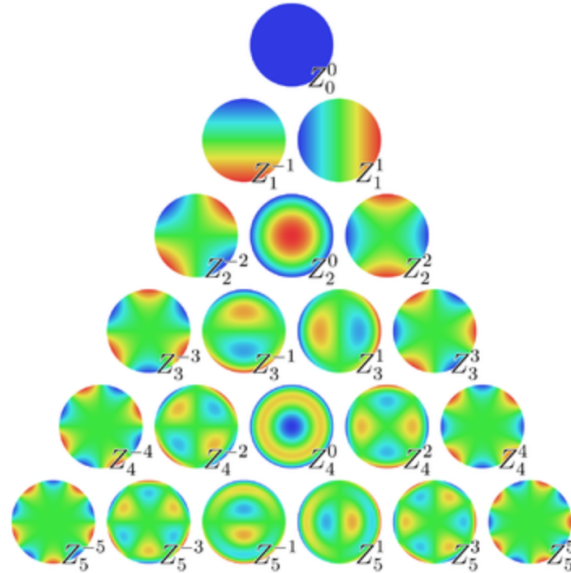

Figure 20: Zernike Polynomials

Different combinations of Zernike polynomials will be used to produce mirror maps in Finesse, which can be seen in Figure 22. Thousands of perturbations will be modeled. Cavity scans will be modeled given each mirror phase map.

However, information about the mirror figure error cannot fully be extracted from the use of Zernike polynomials, and a mirror phase map cannot be reconstructed from the use of Zernike polynomials. Mirror phase maps can be reconstructed from the potential perturbations by using Bayesian inference. A flowchart for the modeling in Finesse can be viewed in Figure 23.
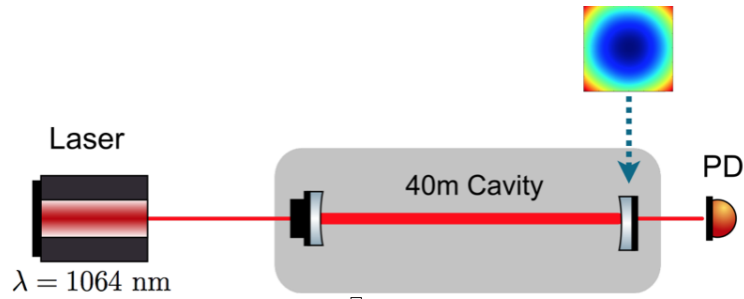
Figure 21: The interferometer as modeled in Finesse, Source: [4]
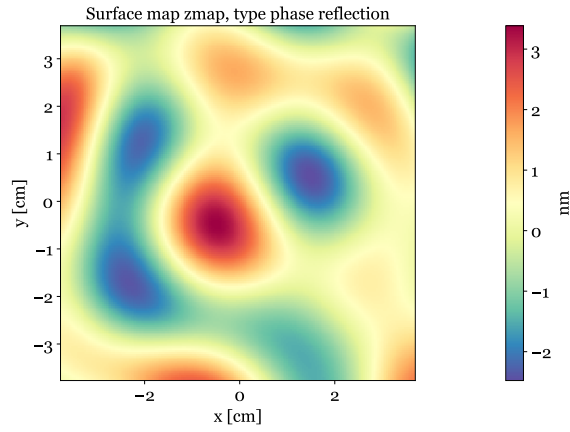

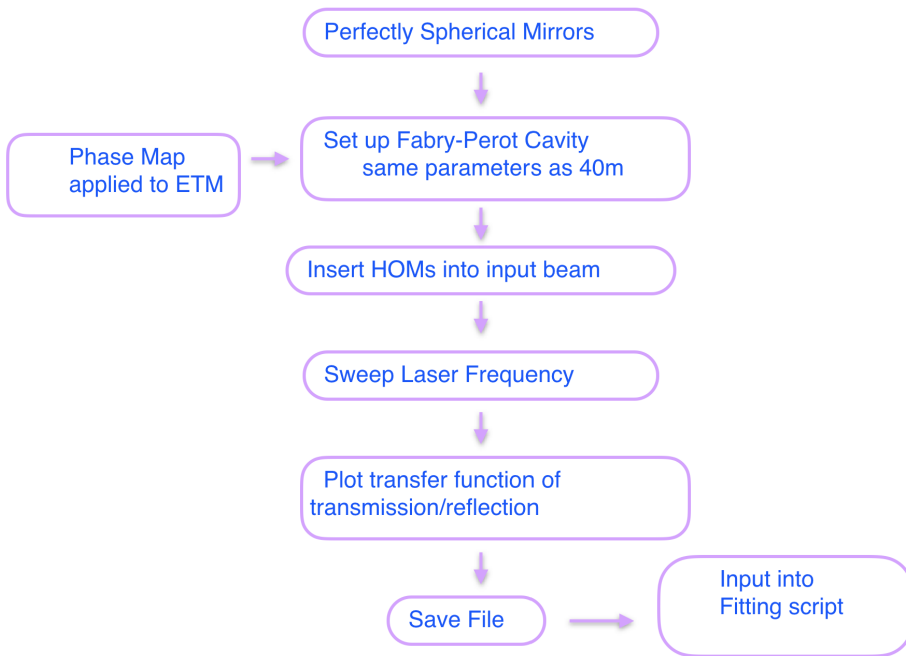Figure 22: A mirror phase map as modeled in Finesse using Zernike polynomials.

Figure 23: Flow Chart showing various stages of Finesse codes to produce mirror phase maps and cavity scans.

7   Bayesian Inference

Bayesian inference will be used to produce the most probable mirror phase maps. The probability of perturbations will be continually updated as more evidence is available. We will use Bayes' theorem of inverse problems, which will be done by analyzing the cavity transmission, then finding the most probable phase map of the cavity mirror for the given cavity scan. Bayesian inference finds the probability of an unknown quantity X, which is the Zernike Polynomials representing the surface imperfections of the ETMY, given the observed measurement Y, which is the cavity frequency scan data.

Bayes' Theorem states that the probability P of X given Y,

$$P\langle X|Y\rangle = \frac{P\langle Y|X\rangle \, P\langle X\rangle}{P\langle Y\rangle} \tag{9}$$

Where X represents the Zernike Polynomials and Y represents data from the cavity scans. Finesse returns: $S(f, Znm)$ which is a function of frequency and Zernike Polynomials. The data from the ith cavity scan is $D_i(f)$. These two quantities are related by frequency.

Thus, Bayes Theorem becomes:

$$P\langle Z|D\rangle = \frac{P\langle D|Z\rangle \, P\langle Z\rangle}{P\langle D\rangle} \tag{10}$$

7.0.1   Markov Chain Monte Carlo

The Markov Chain Monte Carlo method (MCMC) was used in order to extract the posterior probability, which states that the future values do not depend on its previous values [4]. The posterior probability is the probability of a variable after evidence is taken into account.

The finesse model should return a simulated cavity scan $S(f, Z_{nm})$ as a function of Zernike polynomial amplitudes Z_{nm}. Here, Z_{nm} should be understood to be a vector of all Zernike polynomials that should be inferred from the data.

The posterior probability was assumed to have Gaussian noise with a variance of σ^2.

The model for the posterior probability is:

$$p(Z_{nm}|D(f)) \propto exp\left[\frac{-1}{2\sigma^2}\sum_i \int [S(f, Z_{nm}) - D_i(f)]^2 \, df\right] p(Z_{nm}) \tag{11}$$

where $p(Z_{nm})$ is the prior on the amplitudes. The prior is that the amplitudes (and standard deviation) are positive.

The Markov process is run many times in order to create the most probable phase map.

8   Acknowledgements

I would like to thank my mentors Rana Adhikari, Koji Arai, and Gautam Venugopalan for being great teachers and for their guidance.

A special acknowledgement to Rana for giving me this amazing opportunity.

I would like to thank my very supportive co-mentors: Terra Hardwick, Kevin Kuns, Annalisa Allocca, and Jon Richardson for their constant help and encouragement.

A special acknowledgement to Keerthana Nair, my partner for this project, for her support and being a great collaborator.

I would like to thank Alan Weinstein and Alex Urban for their amazing organization of the LIGO SURF program and their enthusiasm and encouragement.

I would like to thank the Caltech SFP program and everyone in the LIGO group for supporting women in STEM.

Special acknowledgement to Martin McHugh at Loyola University for his guidance and initially getting me interested in gravitational waves research.

References

[1] https://www.ligo.caltech.edu/page/ligos-ifo

[2] Kaustubh Singhi, Koji Arai and Rana Adhikari *"Mirror Metrology using Mode Spectroscopy", LIGO-T1700195-v1*

[3] G. Billingsley, H. Yamamoto, and L. Zhang, *Characterization of Advanced LIGO Core Optics.* https://dcc.ligo.org/LIGO-P1700029

[4] Naomi Wharton, Koji Arai and Rana Adhikari, *"Laser Mode Spectroscopy for Mirror Metrology", LIGO-T1700195-v3*

[5] Alberto Stochino, Koji Arai and Rana X. Adhikari, *"A Technique for In-situ Measurement of Free Spectral Range and Transverse Mode Spacing of Optical Cavities". LIGO DCC No. - P1200048*

[6] Kiwamu Izumi, Koji Arai, Bryan Barr, Joseph Betzwieser, Aidan Brooks, Katrin Dahl, Suresh Doravari, Jennifer C. Driggers, W. Zach Korth, Haixing Miao, Jameson Rollins, Stephen Vass, David Yeaton-Massey and Rana X. Adhikari, *"Laser Mode Spectroscopy for Mirror Metrology", LIGO-T1700195-v3*

[7] K. Arai, A. Stochino, R. Adhikari, and the LIGO 40m Lab, *Precise Measurements on Longitudinal and Transverse Mode Spacings of an Optical Cavity using an Auxiliary Laser.* https://dcc.ligo.org/LIGO-G080647

[8] Eric D. Black *"An Introduction to Pound-Drever-Hall Laser Frequency Stabilization"* https://aapt.scitation.org/toc/ajp/69/1

[9] Masaki Ando *"Power recycling for an interferometric gravitational wave detector"*

[10] Anthony E. Sigman *"Lasers"*

[11] MCMC Sampling http://twiecki.github.io/blog/2015/11/10/mcmc-sampling/

[12] Hermite Gaussian Modes https://www.rp-photonics.com/hermite_gaussian_modes.html